Soft Matter

PAPER

View Article Online
View Journal | View Issue

Cite this: *Soft Matter*, 2026, **22**, 1510

The influence of cellular energy status, microtubules, and crowding on mitochondrial motion

Beatrice Corci, [ab] Werner J. H. Koopman, [cde] Amalia M. Dolga [a] and Christoffer Åberg *[a]

Eukaryotic cells rely on a tightly regulated system to transport vesicles and organelles within the cell, as thermal diffusion becomes inefficient for larger cargo. This transport system is composed of the cytoskeleton, a polymer mesh extending throughout the cell, together with different types of motor proteins that attach to and walk along the cytoskeleton, thereby carrying the cargo along with them. Here we used mitochondria in human cells as a model system for cargo transported by motor proteins, followed their motion using microscopy, and analysed the trajectories. Consistent with previous studies, we observed that the mitochondria often remain within a limited region, rattling around, for long periods of time, before finally taking a longer jump. To elucidate the mechanisms behind this behaviour we subsequently perturbed the system. Depletion of cell energy substantially prolonged the waiting time before taking a jump, but also decreased the jump lengths and, to a lesser extent, the extent of the rattling. Disruption of the microtubule network showed a more modest effect on the motion, the largest effect being an approximate doubling of the waiting time before making a jump. Similarly, increasing intracellular crowding by osmotically compressing the cells also had a rather small effect on mitochondrial motion. Again, there was an approximate doubling of the waiting time before making a longer jump, coupled to a more modest decrease in the extent of the rattling. Overall, our data give quantitative insights into the mechanisms underlying motor protein-driven motion and, in particular, highlights the waiting time before making a longer jump as a key parameter.

Received 25th November 2025,
Accepted 18th January 2026

DOI: 10.1039/d5sm01174d

rsc.li/soft-matter-journal

Introduction

A eukaryotic cell is a complex system composed of many different elements, such as macromolecules and organelles, which are often precisely distributed and organised within the cell. While small molecules typically diffuse in the cytosol, eukaryotic cells also have a cell energy-dependent process, motor-protein driven transport across the cytoskeleton, to achieve more efficient transport of larger cargo.[1] For transport along the microtubular part of the cytoskeleton, in particular, organelles and vesicles are transported along an oriented mesh of microtubule fibres (minus ends close to the cell nucleus and plus ends towards the cell periphery), assisted by the motor proteins kinesin (towards plus ends) and dynein (towards minus ends).[2,3] This process, fuelled by the hydrolysis of cell energy in the form of ATP molecules, is thought to ensure a fast and directed transport of cargo.[2]

In the last decade, similarities between the motion within living cells and the one in glassy systems have emerged. The phenomenology of the motion in glassy systems encompasses highly heterogeneous motion, non-Gaussian displacement distributions, and trajectories which can often be described in terms of extended periods of confined 'rattling' interspersed with longer 'jumps'.[4,5] Such a behaviour has been observed in a variety of living organisms, including bacteria,[6] yeast,[7] human cells,[8] and plant cells.[9] Previously, we have observed that mitochondria in a range of cell types also display a motion analogous to that in glassy systems.[10]

To understand in more detail the nature of intracellular motion, a common approach is to perturb the system. In the case of motor protein-driven motion, this is typically achieved

[a] *Groningen Research Institute of Pharmacy, University of Groningen, Antonius Deusinglaan 1, 9713 AV Groningen, The Netherlands. E-mail: christoffer.aberg@rug.nl*
[b] *Zernike Institute for Advanced Materials, University of Groningen, Nijenborgh 3, 9747 AG Groningen, The Netherlands*
[c] *Department of Pediatrics, Amalia Children's Hospital, Radboud University Medical Center, Nijmegen, The Netherlands*
[d] *Radboud Center for Mitochondrial Medicine, Radboud University Medical Center, Nijmegen, The Netherlands*
[e] *Human and Animal Physiology, Wageningen University & Research, Wageningen, The Netherlands*

by depleting cell energy[11–13] or disrupting the cytoskeleton.[11–14] Such alterations can be achieved by exposure to chemical compounds that suppress ATP synthesis[15] or microtubule stability.[16] Besides factors directly involved in motor protein-driven motion, crowding within the cell is another potential mechanism that could affect the transport. Indeed, eukaryotic cells are composed of macromolecules and organelles occupying 5–40% of the volume.[17] Against this background, it has been posited that the dense nature of the cytosol can interfere with cell physiology[18] and slow down intracellular motion due to physical constraints.[19,20]

For their biological relevance and transport mechanism, mitochondria are a very suitable endogenous probe to explore intracellular motion.[13] These organelles, present in virtually all eukaryotic cells, play a role in many essential processes.[21,22] While their shape and distribution depends on cell type,[23] in many cells the majority of mitochondria are found highly interconnected in a network with the remaining mitochondria detached from the network.[24,25] While network remodelling occurs through fission and fusion events,[26,27] the detached mitochondria are moved around the cytosol by motor proteins.[28–33]

Here we used these characteristics of mitochondria to study the effect of different perturbations on the motion of detached mitochondria. Using live-cell imaging, we recorded mitochondria moving inside cells, determined their trajectories, and analysed their motion. Our results demonstrate that mitochondrial motion is negatively affected by cell energy depletion, by microtubule disruption, and upon cell crowding, albeit to different extents and in different manners. Moreover, we are able to quantify these changes in the motion, giving more detailed insights into the nature of intracellular motion in general, and of mitochondria in particular.

Experimental

Cell culture

HEK 293 (American type culture collection, ATCC; no. CRL-1573, lot no. 63966486) cells were cultured in Dulbecco's Modified Eagle's Medium (DMEM; Gibco, Life Technologies, Eugene, OR, USA), with 4.5 g L^{-1} D-glucose, 1.1 g L^{-1} of pyruvate, 8.62 g L^{-1} of L-glutamine and supplemented with 10% (v/v) foetal bovine serum (FBS; Gibco, Life Technologies, Eugene, OR, USA). The cells were kept in a 37 °C and 5% CO_2 incubator and were subcultured twice per week. Cells were used between passage 3–24.

Stably transfected Flp-in T-Rex293 cells (derived from HEK 293 cells) conditionally expressing the green fluorescent protein AcGFP1 fused to the mitochondrial-targeting sequence cox8 were cultured in DMEM supplemented with 10% (v/v) FBS, 1% (v/v) pen/strep (Thermo Fisher, Waltham, MA, USA), hygromycin 200 μg mL^{-1} (Thermo Fisher, Waltham, MA, USA), and blasticidin 50 μg mL^{-1} (Gibco, Thermo Fisher, Waltham, MA, USA). The cells were kept in a 37 °C and 5% CO_2 incubator and subcultured twice per week. To induce the expression of AcGFP1, doxycycline 1 μg mL^{-1} (Sigma Aldrich, St. Louis, MO, USA) was added to the medium for 24 h. Cells were used between passage 8–15.

Regular mycoplasma tests were carried out for both cell lines. All experiments presented here are from mycoplasma negative cells.

Cell treatment and mitochondrial staining

Experiments were conducted 48 h after cell seeding. For experiments on HEK 293 cells, 60 000 cells were seeded into μ-slide 8 glass bottom wells (Ibidi, Gräfelfing, Germany). To decrease ATP levels, cells were treated with sodium azide (Sigma Aldrich, St. Louis, MO, USA) by preparing a 50 mg mL^{-1} solution of sodium azide in cell culture medium and adding it to the wells already containing cell culture medium to reach a final sodium azide concentration of 5 and 10 mg mL^{-1}, respectively, after which the cells were incubated for 3 h at 37 °C and 5% CO_2. Microtubule depolymerization was induced by treating the cells with nocodazole (Biovision, CA, USA) in DMEM at a final concentration of 5 μM and 10 μM for 4 h.

For mitochondria visualisation, cells were stained with MitoTracker Deep Red (Invitrogen, Waltham, MA, USA) diluted in transparent live cell imaging solution (Invitrogen, Waltham, MA, USA) at 200 nM, after which the cells were incubated for 25 min at 37 °C and 5% CO_2. Mitochondria were stained after any eventual cell treatments and cells were directly imaged after the staining incubation. For experiments on fixed cells, cells were first stained with MitoTracker Deep Red, as described above, and later fixed with 4% paraformaldehyde for 15 min at room temperature.

For experiments with AcGFP1-expressing HEK 293 cells, 200 000 cells were seeded into glass bottom microwell Petri dishes (MakTek, Ashland, MA, USA) for 48 h. To observe the effect of crowding, cells were treated with D-sorbitol (Merk, Darmstadt, Germany), by adding a 5 M solution of sorbitol in Phosphate-Buffered Saline (PBS) to the Petri dish already containing cell medium to reach a final concentration of 550 mM sorbitol. As a control, the same procedure was applied using only PBS (without sorbitol). The cells were observed under the microscope before and after the treatment.

ATP bioluminescence assay

In order to measure ATP levels, 900 000 HEK 293 cells were seeded into 6-well plates. After 24 h, they were treated with sodium azide (as described above). After removing the medium to collect eventual dead cells, the remaining cells were harvested in 1 mL of PBS. Next, 200 000 cells per condition were resuspended in 200 μL SONOP buffer [70% (v/v) ethanol containing 2 mM EDTA at pH 10.9] and left in it for 2–3 min. The ATP luciferase enzyme (ATP assay kit, Roche, Basel, Switzerland) was added in a 1 : 1 volume ratio to the cell suspensions in a black 96-well plate. Luminescence was quantified using a SpectraMax iD3 microplate reader (Molecular Devices, San Jose, CA, USA).

Microtubule immunostaining

To visualise the microtubule network, HEK 293 cells were (after nocodazole treatment, as described above, or in the absence of

nocodazole treatment, in the case of the control) fixed with 4% paraformaldehyde for 15 min at room temperature. Subsequently, the cells were permeabilized with 0.1% (v/v) Triton X-100 for 5 min at room temperature. A 1 h exposure (at room temperature) to a blocking solution (9 mL PBS + 30 μL Triton-X-100 + 500 μL FBS) was done prior to staining. Then, exposure to α-tubulin antibody (#3873; Cell Signaling Technology, Danvers, MA, USA) was done overnight at 4 °C, followed by an additional 1–2 h of exposure (room temperature) to the anti-rabbit AlexaFluor 488-conjugated secondary antibody (Invitrogen, Waltham, MA, USA). The cells were then left for 5 min at room temperature with DAPI (4′,6-diamidino-2-phenylindole) at 1 μg mL^{-1} in PBS to stain the cell nuclei. Images were acquired with a Zeiss Celldiscoverer 7 confocal microscope using a 405 (DAPI) and a 488 nm (AlexaFluor 488) diode excitation laser, and a quadruple band pass filter (425/30; 514/30; 592/25; 709/100 nm).

Cell area assessment

To assess the size of the cells, brightfield microscopy was performed on AcGP1-expressing HEK 293 cells both on control cells (not treated with anything), negative control cells (cells treated with PBS) and crowded cells (cells treated with 550 mM sorbitol). Timelapses were recorded every 5 s for 10 min with a Zeiss Celldiscoverer 7 microscope. To determine the cell area, ImageJ[34] was used to manually draw a region of interest around individual cells with the 'polygon selection' tool and thereby quantify the area. The same approach was used to measure the area of cells under all three different conditions.

Live-cell imaging

Cells were observed with a Zeiss Celldiscoverer 7 confocal laser scanning microscope, equipped with an Airyscan unit (Zeiss, Oberkochen, Germany) using a water immersion 50× objective (numerical aperture 1.2, magnification changer 1×). Images were acquired every 300 ms (350 ms for the AcGFP1-expressing cells) for 3 min. To visualise MitoTracker Deep Red-labelled mitochondria, a 640 nm diode excitation laser and a quadruple band pass filter (425/30; 514/30; 592/25; 709/100 nm) were used. To visualise GFP-labelled mitochondria, a 488 nm diode excitation laser and the same quadruple band pass filter were used. Cells were kept at 37 °C and 5% CO_2 during microscopy.

Organelle tracking

Cells showing signs of phototoxicity were not analysed. Single punctate mitochondria were tracked using the Fiji[35]/ImageJ[34] plugin TrackMate[36,37] (version 7.10.2) as previously described.[10] Briefly, a region of interest was selected to focus on a single or multiple mitochondria. Their trajectories were automatically determined with the software and subsequently manually checked to avoid potential misidentification.

Trajectory analysis

The analysis procedure followed that of our previous work.[8,10] As a starting point, for each trajectory the square displacement, Δr^2, was calculated (in two dimensions) between all pairs of time points for which the trajectory was defined. This data was binned by lag time, using bins based on the average acquisition rate. The time-averaged mean square displacement for individual trajectories was subsequently calculated by averaging over lag time. The time- and ensemble-averaged mean square displacement was calculated by another averaging over all acquired trajectories.

The displacement distribution was obtained from the same square displacements, by taking the square root to form the displacement, Δr, then grouping all displacements by lag time and pooling all trajectories together. For each lag time, a histogram of displacements was calculated, normalised by the total number of displacements and bin size (meaning that its integral over Δr was 1). Finally, the histogram was divided by $2\pi\Delta r$ to exclude the effect of the two-dimensional geometry.

A two-dimensional version[8] of the model developed by Chaudhuri *et al.*[4,38] (see previous literature[8] for the somewhat lengthy expressions) was fitted to the experimentally determined displacement distributions. The model was fitted to the logarithm of the distribution with 4 free parameters (l, d, τ_1, and τ_2; see main text for their definition) and for all lag times simultaneously (a global fit). The errors on the fitting parameters were determined as the square root of the diagonal elements of the covariance matrix of the parameters.

The distribution of waiting times before a mitochondrion moved a given distance for the first time and the waiting time before it moved the distance a subsequent time was determined as proposed by Wang *et al.*[39] For all trajectories, all 'subtrajectories' formed from the original trajectory by varying the starting point along the trajectory were considered. However, only subtrajectories lasting at least 10 s and only the first 10 seconds of those subtrajectories were considered to avoid bias (see Wang *et al.*[39] for a discussion of this point). The first waiting time was then determined as the first time a mitochondrion moved a given distance along the subtrajectory; any (potential) subsequent move the same distance, starting from the previous time the mitochondrion moved the given distance, was used to determine the subsequent waiting times. A histogram of waiting times was calculated using logarithmically-sized bins, normalised by both the total number of sampled waiting times as well as the bin width (not the logarithm of the bin width). This normalisation results in the probability density function for the waiting time, aside from that the procedure for determining the waiting times[39] has an upper limit (10 s in our case); because of this, the normalisation with the total number of samples is not quite accurate, but the distribution will nevertheless carry most of the statistical weight.

Results and discussion

Model system and approach

As a model system to investigate the effect of perturbations on motor protein-driven intracellular motion, we followed the motion of mitochondria in Human Embryonic Kidney (HEK) 293 cells. Mitochondria move on the microtubule network by

motor proteins, being carried by kinesin motor proteins towards the plus ends (typically towards the cell periphery) and by dynein motor proteins towards the minus ends (typically towards the cell body).[29,40,41] To localise the mitochondria inside the cells, we fluorescently labelled them with a commercially available probe (MitoTracker Deep Red); in some experiments we instead used HEK 293 cells expressing a green fluorescent protein (AcGFP1) fused to a mitochondrial-targeting sequence (cox8) for labelling.[42,43]

To follow the labelled mitochondria in time, images were recorded using live-cell confocal microscopy. Two-dimensional time lapses were acquired every 300 ms (350 ms for the AcGFP1-expressing cells) for 3 min, resulting in 600 frames (515 frames) in total, using a pixel size of 120 nm for a total image size of $58.79 \times 58.79\ \mu m^2$ (488×488 pixels). See Fig. 1 and Movie S1 for an example. These settings largely avoided inducing phototoxicity to the cells, but if a response was observed (*e.g.*, the cell shrinking and/or the mitochondrial network rapidly changing shape) then the field of view was not analysed.

While most mitochondria form a network inside the cell, some mitochondria remain punctate and detached from the network (Fig. 1; arrows). We focussed on these detached mitochondria, as we considered them more appropriate as examples of motor protein-driven motion,[10,13] and determined their trajectories as described in the Experimental section. The majority of mitochondria are not in the vicinity of the (outer) cell membrane, so we do not expect boundary effects to be important.[44] While the detached mitochondria were easier to track, the tracking procedure nevertheless remains challenging due to the two-dimensional acquisition and the presence of a dense mitochondrial network. Therefore, a distribution of trajectories of different lengths was obtained (Fig. S1–S3).

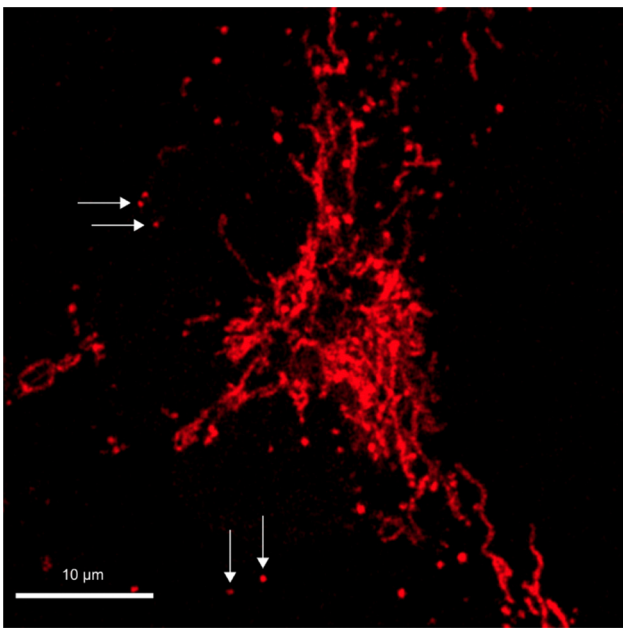

Fig. 1 Mitochondria in HEK 293 cells. Mitochondria in HEK 293 cells were fluorescently labelled with MitoTracker Deep Red and observed live using confocal microscopy. The punctuate (or spot-like) detached mitochondria (some examples indicated by arrows) were subsequently tracked as described in the Experimental section. See Movie S1 for the time series.

As a control, we exposed the cells to an agent that crosslinks the intracellular proteins, stopping most dynamic events but still preserving cellular structure (fixed cells). The mitochondria were subsequently followed in these cells and we evaluated their ensemble- and time-averaged mean square displacement. It exhibits a plateau up to 30–40 s, with an increase at a longer timescale of around 100 s (Fig. S4). We interpret the plateau to represent the finite precision with which we can localise a mitochondrion, in which case the intercept represents (due to the two dimensions) 4 times the localisation precision squared;[45,46] the lowest value 0.00231 μm^2 then corresponds to a localisation precision of $\sqrt{0.00231\ \mu m^2/2} = 0.024\ \mu m$. Furthermore, the increase at longer times is presumably due to a small drift of the microscope stage which is difficult to completely prevent at these timescales (the mean square displacement after 180 s is 0.0158 μm^2, which corresponds to an average drift of only $\sqrt{(0.0158 - 0.00231)\ \mu m/180\ s} = 0.7\ nm\ s^{-1}$). As will transpire below, this increase at longer times is completely negligible compared to all results for the mean square displacement of mitochondria in living cells (Fig. S5).

To gauge the level of reproducibility of the approach, we took advantage of the fact that we acquired two different datasets of mitochondria in unperturbed HEK293 cells (one for the experiments on cell energy depletion and the other for the experiments on microtubule disruption) and compared their ensemble- and time-averaged mean square displacement (Fig. S6). Although not completely identical, the mean square displacement from these two datasets are in good agreement, especially at short time scales (Fig. S6). The extent of such differences should be kept in mind when considering the effect of the perturbations we perform on the cells in what follows.

Cell energy depletion

We started by characterising the effect of cell energy depletion on mitochondrial motion. Indeed it is known that a lack of cell energy results in a slowing down of active motion.[13,47–49] To this end we used sodium azide (NaN_3), a compound that inhibits the respiratory chain enzyme cytochrome *c* oxidase (on the mitochondrial inner membrane), causing a decrease in ATP production.[15,50] As mitochondria produce cell energy, it should be acknowledged that perturbing cell energy production may, aside from the lowered amount of cell energy available, directly affect them as the cell attempts to counteract the depletion. Nevertheless, as will transpire below, the effect of cell energy depletion on mitochondrial organisation and motion was fairly moderate under the conditions we applied. Moreover, the fluorescent stain we used to label the mitochondria only labels the metabolically active mitochondria,[51] so the (subpopulation of) mitochondria we analysed should behave normally, aside from the depletion of cell energy whose effect we are interested in.

Cell energy was depleted by exposing the cells to 5 and 10 mg mL^{-1} of sodium azide for 3 h. Upon cell energy-depletion, the cells gradually changed shape and shortened

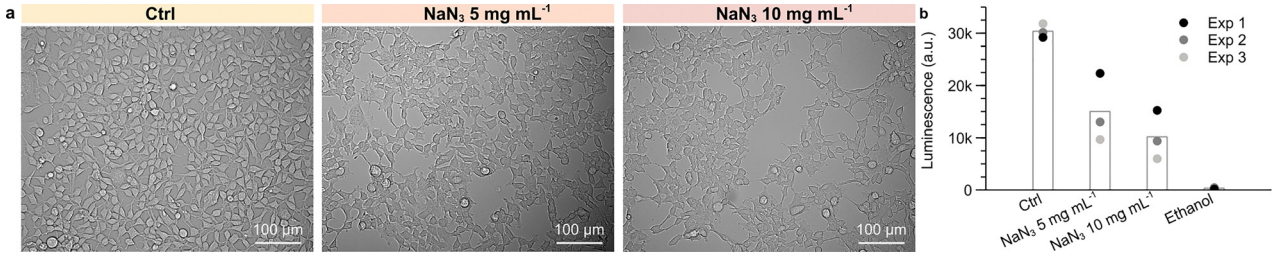

Fig. 2 Cell energy depletion in HEK 293 cells. (a) Brightfield images of cells *not* subjected to ATP depletion (Ctrl) and of cells subjected to ATP depletion by being exposed for 3 h to 5 and 10 mg mL^{-1} sodium azide (NaN_3). (b) ATP quantification of cells after cell energy depletion. The same number of cells were measured under all conditions and most dead cells were removed during sample preparation (see Experimental section for details), so the results should be interpreted as the amount of ATP per living cell. Cells exposed to 70% ethanol for 30 min were used as a positive control. The bars represent the mean over three independent experiments, with the symbols representing the mean over duplicates for each individual experiment.

their protrusions, showing less interconnected cell networks than unperturbed cells (Fig. 2a). To measure the degree of cell energy decrease, we quantified ATP levels by luminescence (Fig. 2b). In the presence of sodium azide, ATP levels decreased in a concentration-dependent manner, roughly halving at a concentration of 5 mg mL^{-1} and decreasing to around a third at a concentration of 10 mg mL^{-1}. To assess the effect of cell energy depletion on mitochondrial organisation, we also performed an (illustrative) analysis of the network structure from the microscopy images (Supplementary methods) which shows that the mitochondrial network undergoes some structural changes upon cell energy depletion (Fig. S7). As a further decrease of ATP levels may cause the cells to counteract the lack of cell energy by various processes, we used the conditions illustrated here to evaluate the influence of decreasing ATP levels on mitochondrial motion.

We thus tracked the detached (as opposed to the network-forming) mitochondria in time under both unperturbed and cell energy-depleted conditions (see Fig. S1 for trajectory length distributions). Qualitative inspection of their trajectories already gives an idea of how the motion changes under the different conditions (Fig. 3a). In unperturbed cells, mitochondria alternate moments of rattling (moving within a limited region) with longer jumps of a few micrometres, the latter often with a unidirectional character (Fig. 3a; Ctrl). Upon cell energy depletion, mitochondrial motility gradually decreased. For mitochondria in cells with halved cell energy (Fig. 3a; NaN_3 5 mg mL^{-1}), the trajectories are dominated by small rattling movements and a few longer jumps; these jumps become increasingly rare as cell energy is further depleted (Fig. 3a; NaN_3 10 mg mL^{-1}).

For a more quantitative analysis, we evaluated the mean square displacement as a function of time, first for individual trajectories where the averaging is over lag time (Fig. 3b). In unperturbed cells, mitochondria exhibit highly heterogeneous behaviour with quite different displacements over time (Fig. 3b; Ctrl). However, upon cell energy depletion, the heterogeneity of the trajectories is noticeably reduced (Fig. 3b; NaN_3 5 and 10 mg mL^{-1}) with mitochondria behaving more similarly and moving shorter distances as cell energy is reduced more.

The decrease in overall motion is more evident in the ensemble- and time-averaged mean square displacement (Fig. 3c). Mitochondria in unperturbed cells show a mean square displacement that grows roughly as a power law up to around 20 s (Fig. 3c; Ctrl) in a superdiffusive fashion (*cf.* the two solid lines in Fig. 3c representing diffusive and ballistic behaviour, respectively). At longer timescales the mean square displacement appears to level off but it should be noted that statistics is limited here. Upon halving of cell energy (Fig. 3c; NaN_3 5 mg mL^{-1}) the mean square displacement exhibits a slower rate of growth, in particular at shorter timescales. Upon further decrease of cell energy (Fig. 3c; NaN_3 10 mg mL^{-1}) the mean square displacement at subsecond timescales grows even slower. Given the proximity of these results to those from immobilised mitochondria (Fig. 3c; Fixed cells) we cannot unequivocally confirm the presence of an apparent plateau; however, our previous results using a different experimental set-up,[10] where the localisation precision was better, hint at it being real (Fig. S8). Regardless, even upon the stronger energy depletion (Fig. 3c; NaN_3 10 mg mL^{-1}) the mean square displacement nevertheless starts to grow more rapidly at longer timescales.

To better characterise the effect of cell energy-depletion on the motion, we next calculated the displacement distribution at timescales of 0.6–3 s (Fig. 4, data points). Mitochondria in unperturbed cells exhibit a non-Gaussian displacement distribution, from which we observe that the majority of mitochondria move only short distances $\sim$0.05–0.10 µm and that only a few of them move further than 0.10 µm (Fig. 4a; note the log-scale). As cell energy is reduced, the probability of a mitochondrion moving longer distances decreases, while the probability that the mitochondrion remains at a similar position increases accordingly (Fig. 4b and c). In unperturbed cells, the mean square displacement grows approximately as a power law up to 20 s (Fig. 3c; Ctrl); interestingly, using the exponent of this power law to rescale space makes the displacement distributions roughly collapse to a universal function (Fig. S9). The situation is less clear for cell-energy-depleted cells, where the mean square displacement cannot be represented by a single power law, even approximately (Fig. 3c; NaN_3 5 and 10 mg mL^{-1}).

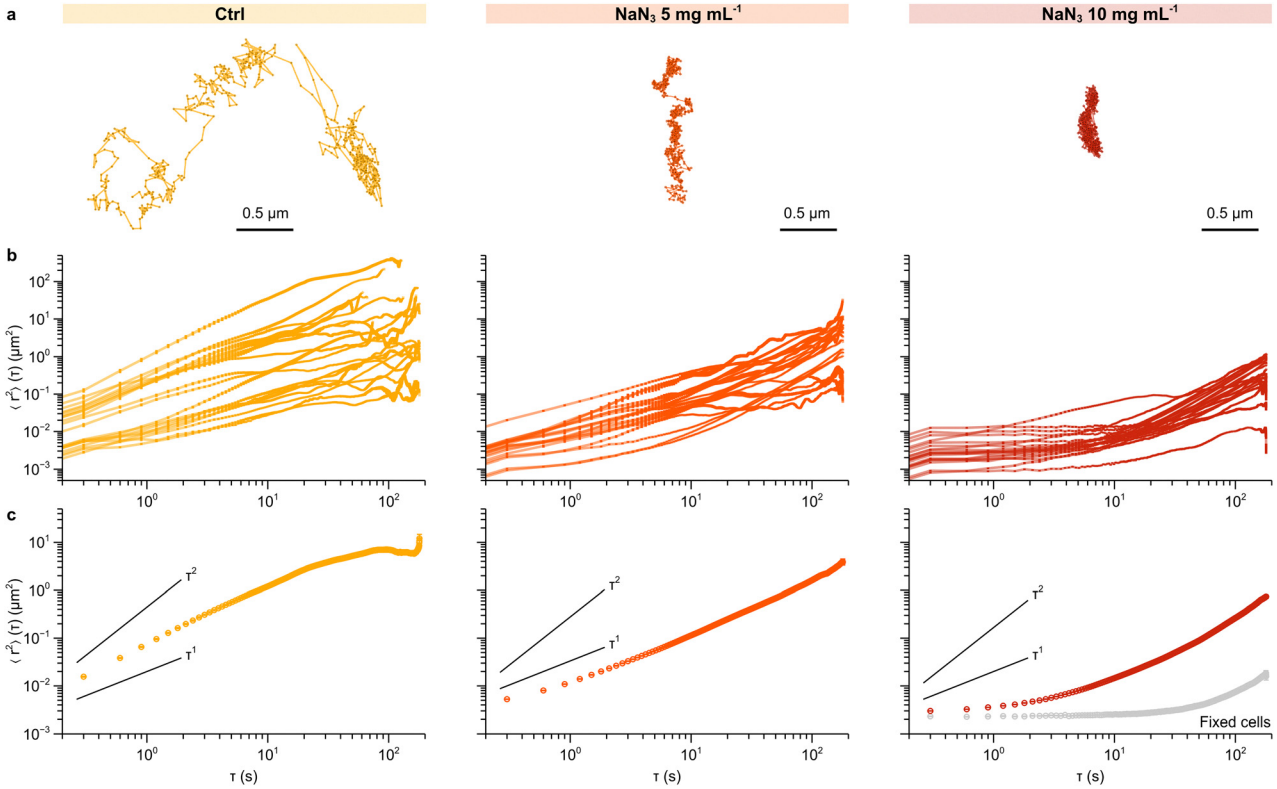

Fig. 3 Mean square displacement of mitochondria in cell energy-depleted HEK 293 cells. The results are shown for control cells (not depleted of cell energy), together with cells depleted of cell energy by exposure to 5 and 10 mg mL^{-1} sodium azide (NaN_3). (a) Representative examples of mitochondrial trajectories. (b) Time-averaged mean square displacement of 20 random mitochondrial trajectories as a function of lag time, τ. Error bars represent standard error of the mean. (c) Ensemble- and time-averaged mean square displacement of mitochondria. Error bars represent standard error of the mean (most of them too small to be visible). Solid lines represent diffusive motion (proportional to τ) and ballistic motion (proportional to τ^2), respectively, as a guide to the eye. Mitochondrial trajectories in fixed cells (grey) were used as a control.

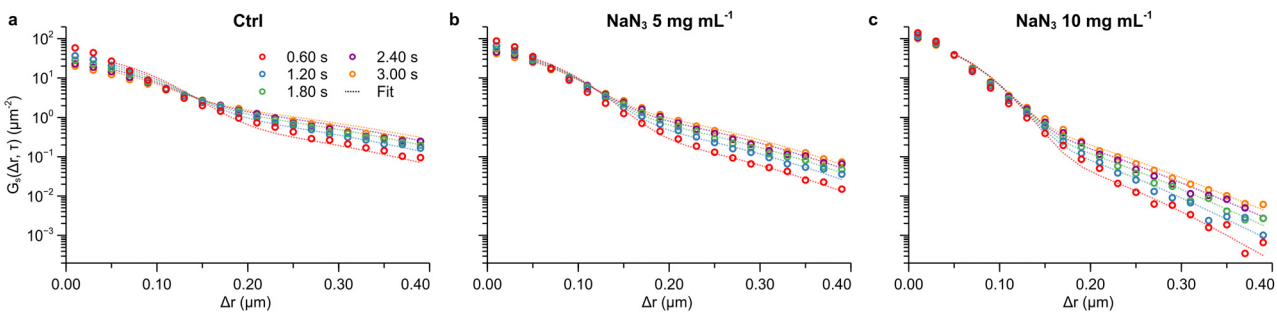

Fig. 4 Displacement distribution of mitochondria in cell energy-depleted HEK 293 cells. Displacement distribution in (a) control cells (not depleted of cell energy), together with cells depleted of cell energy by exposure to (b) 5 mg mL^{-1}, and (c) 10 mg mL^{-1} sodium azide (NaN_3) for 3 h. A previously presented model describing the motion in several glassy systems[4,38] was globally fitted to the data for displacements larger than 0.05 μm (dashed lines) with the resulting fitting parameters reported in Table 1 and Table S1.

To extract more information we instead fitted a mathematical model to the displacement distribution. Given the tendency of mitochondria to often remain (fairly) stationary for extended periods of time before moving longer distances (Fig. 3a) we have previously suggested that viewing the motion of mitochondria as glassy may be fruitful.[10] We stress that we do not wish to imply that the motion of mitochondria is identical to that in a glass – for example, the jumps appear less instantaneous – but rather that it is a useful analogy. From this perspective, it is convenient that Chaudhuri *et al.*[4,38] have shown that a simple mathematical model describes the displacement distribution in several glassy systems very well, including that in simulations of a silica melt,[52,53] simulations of a binary Lennard-Jones system,[54] a colloidal hard sphere glass,[55] an attractive colloidal gel,[38] and a driven granular system.[56] Their model is, indeed, based on the notion that

objects spend much of their time rattling around within a confined area, before taking a longer jump.

In mathematical terms their model, which we have previously[8] translated into the two dimensions appropriate for the experiments described here, is based on a continuous time random walk formalism.[57,58] Thus we describe the rattling around in terms of a Gaussian displacement distribution with a characteristic length l, *viz.* $(2\pi l^2)^{-1}\exp(-r^2/2l^2)$. Similarly, we describe the extent of the jumps in terms of another Gaussian distribution, $(2\pi d^2)^{-1}\exp(-r^2/2d^2)$, now with characteristic length, d. The time an object spends rattling around before taking a jump, the waiting time, is more involved. First, when applying the continuous time random walk formalism to glassy systems, one has to make a distinction between the first waiting time, that is, the time an object waits from the start of the observation time until the first time it makes a jump, and any of the subsequent waiting times. Second, both of the waiting time distributions are in reality highly non-trivial. However, Chaudhuri *et al.* argue[38] that in practical terms it is possible to progress by assuming that both waiting times are exponentially distributed, *viz.* ${\tau_1}^{-1}\exp(-\tau/\tau_1)$ and ${\tau_2}^{-1}\exp(-\tau/\tau_2)$. Here τ_1 and τ_2 are the characteristic times for the first and subsequent jumps, respectively, and to reflect their interpretation in terms of first and subsequent waiting times it must hold that $\tau_2 < \tau_1$. We have previously demonstrated[8,10] that this model provides a good description of the displacement distribution inside cells of several different objects, including mitochondria, in multiple cell types, including the HEK 293 cells used here.

We thus fitted this model to the present results, only fitting to distances larger than 0.05 μm (corresponding to the mean square displacement in fixed cells; Fig. S4). As expected this model fits the motion of mitochondria in unperturbed cells well (Fig. 4a, dashed lines), but it also fits the data for cells with lowered cell energy well (Fig. 4b and c, dashed lines). While one should not attach absolute significance to the fitting parameters extracted from such fits, the fitting parameters are nevertheless useful as a quantitative means of assessing how cell energy-depletion affects the motion (Table 1). We observe that the waiting time before making a first jump, τ_1, increases substantially as cell energy levels decrease, which within the model would mean that the lower cell energy, the longer a mitochondrion has to wait before making a first jump. The waiting time for subsequent jumps, τ_2, was not well-determined from the fits (Table S1) so we will not discuss it further. The extent of the rattling, l, and the distance covered during a jump, d, decrease as cell energy is depleted (Table 1). This is particularly true for the jumps, d, which at the lowest cell energy level we tested was reduced to almost half of the length under unperturbed conditions.

Table 1 Parameters describing mitochondrial motion in cell energy-depleted HEK 293 cells. The parameters were extracted by fitting a previously presented model describing the motion in several glassy systems[4,38] to the displacement distribution (Fig. 4). This model is based on four different parameters: τ_1, the time before a first jump; τ_2, the time before any subsequent jump; l, the size of the rattling; and d, the size of a jump. The time before a subsequent jump, τ_2, was not well-determined from the fits and has been excluded to avoid confusion (for completeness it may be found in Table S1)

Condition	τ_1 (s)	l (μm)	d (μm)
Control	3.35 ± 0.20	0.063 ± 0.002	0.147 ± 0.011
5 mg mL^{-1} NaN_3	8.10 ± 0.41	0.056 ± 0.001	0.118 ± 0.004
10 mg mL^{-1} NaN_3	35.46 ± 3.11	0.045 ± 0.001	0.080 ± 0.003

The above analysis depends on the model borrowed from glassy dynamics, which, while useful, is not completely appropriate to describe intracellular motion. To complement the results on the waiting times, we also performed a model-independent characterisation. Thus, we calculated how long it took the mitochondria to move a given distance for the first time, and how long it took to move the same distance any (potential) subsequent time, directly from the trajectories (for further details about the procedure see Experimental section). The calculation was done for different distances starting from 0.15 μm, which is roughly the extent of a jump performed by mitochondria in unperturbed cells extracted from the fitting (Table 1, d). For all cases shown here and for all distances defining the waiting time, the distribution before moving the distance the first time does not overlap with the waiting time before moving the distance a subsequent time (Fig. 5; *cf.* blue and orange symbols). This 'decoupling', a feature of glassy dynamics,[59,60] is something we previously observed for several different objects moving in several different cell types.[8,10]

Even if decoupling is preserved across all conditions, the distributions do change upon cell energy depletion. Clearly, the stronger the cell energy depletion, the longer a mitochondrion waits before moving the distance a first time (Fig. 5; blue) but also before moving the distance a subsequent time (Fig. 5; orange), and this is more prominent the longer the distance considered. Furthermore, in the more extreme scenarios (larger energy-depletion and/or long distances) the probability that a mitochondrion moves the distance in a short time decreases to such a large extent that there is the formation of a 'peak' at longer waiting times around 3.7 s (Fig. 5c; last column).

In summary, we observed that decreasing cellular energy levels causes a decrease in overall mitochondrial movement and mitochondria increasingly spend most of the time rattling around, waiting longer before taking a (unidirectional) jump. In interpreting these results we note that for both kinesin and dynein the taking of one step along a microtubule is tied to ATP hydrolysis.[61] It should also be kept in mind that typically multiple motors, of both types, attach to the same vesicle.[62] Regardless, even when cell energy is depleted the extent of the rattling is larger than a single step, suggesting that cell energy depletion, rather than completely stopping individual steps, makes processive runs less likely. Another effect to keep in mind, though, is that cell energy depletion also diminishes fluctuations of the cytoskeleton, fluctuations which can also drive motion.[12,63]

Microtubule perturbation

As a second factor involved in the motion of the mitochondria, we considered the cytoskeleton. With regards to the actin part

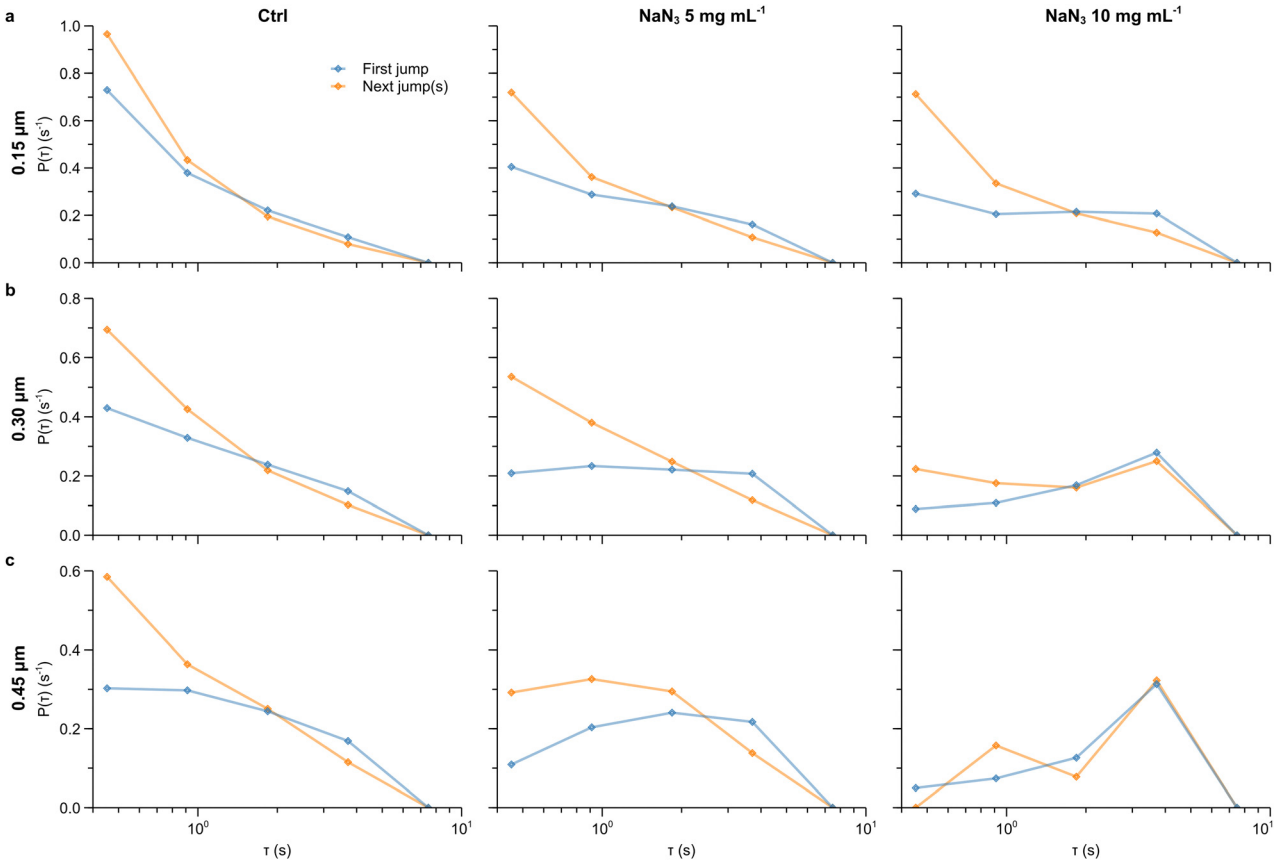

Fig. 5 Waiting time distributions of mitochondria to move a given distance in cell energy-depleted HEK 293 cells. The time before moving a certain distance the first time (blue) and any subsequent time (orange) was evaluated for distances of (a) 0.15 μm; (b) 0.30 μm; and (c) 0.45 μm. The results are presented in terms of the normalised probability density function of the two times. Note the log scale. The calculations were limited to the first 10 s only (see Experimental section for details).

of the cytoskeleton, the myosin motor protein Myo19[64] has recently been shown to bind to mitochondria[65] and to move them along the actin network in filopodia of HeLa cells.[66] The actin network also contributes to mitochondrial fission,[67–69] mitochondrial dynamics during cell division,[65,70] and cell migration.[71,72] Nevertheless, for long distance movement of mitochondria, the microtubule network remains the more important mode of transport.[29] Furthermore, we avoided investigating dividing and moving cells. For these reasons we focused on the microtubule part of the cytoskeleton.

In order to disrupt the microtubule network, we exposed the cells to nocodazole, an anticancer drug,[73,74] at concentrations of 5 and 10 μM for 4 h. To assess whether the microtubule network was thereby broken down, the cells were observed using brightfield microscopy (Fig. 6a) and the α-tubulin subunit of microtubules was fluorescently labelled using immunostaining (Fig. 6b). Unperturbed cells spread out on the substrate (Fig. 6a; Ctrl) and the presence of long microtubule fibres can be observed throughout the cells (Fig. 6b; Ctrl). After nocodazole exposure, however, the cells spread out less (Fig. 6a; Nocodazole 5 and 10 μM) and microtubules are no longer visible or are much shorter (Fig. 6b; Nocodazole 5 and 10 μM). There are also fewer cells after nocodazole exposure (Fig. 6a; Nocodazole 5 and 10 μM), probably because the lack of a microtubule network makes the cells attach less well to the substrate, causing them to be removed when the cell medium is exchanged during the experimental procedure. While there is a clear difference between cells exposed or not exposed to nocodazole, there is no major difference between the two concentrations of the compound (aside from that possibly more cells detach at 10 μM), implying that exposure of 5 μM nocodazole for 4 h is sufficient to disrupt the microtubule network. We also performed an (illustrative) analysis of the effect of microtubule network disruption on mitochondrial organisation (Fig. S10). In general, the effect is not very pronounced, though after microtubule disruption the mitochondrial network tends to be more branched and the mitochondria appear to be larger after exposure to 5 μM nocodazole. Even if the microtubule damage looks similar for the two nocodazole concentrations, both were considered for further analysis on the motion to verify a possible difference in the overall dynamics.

To observe mitochondrial motion after microtubule impairment, microscopy and tracking of mitochondria were performed following the same procedure as above (Fig. S2 shows the trajectory length distributions). Note that, compared to cell energy depletion (Fig. 3–5) new data were collected for

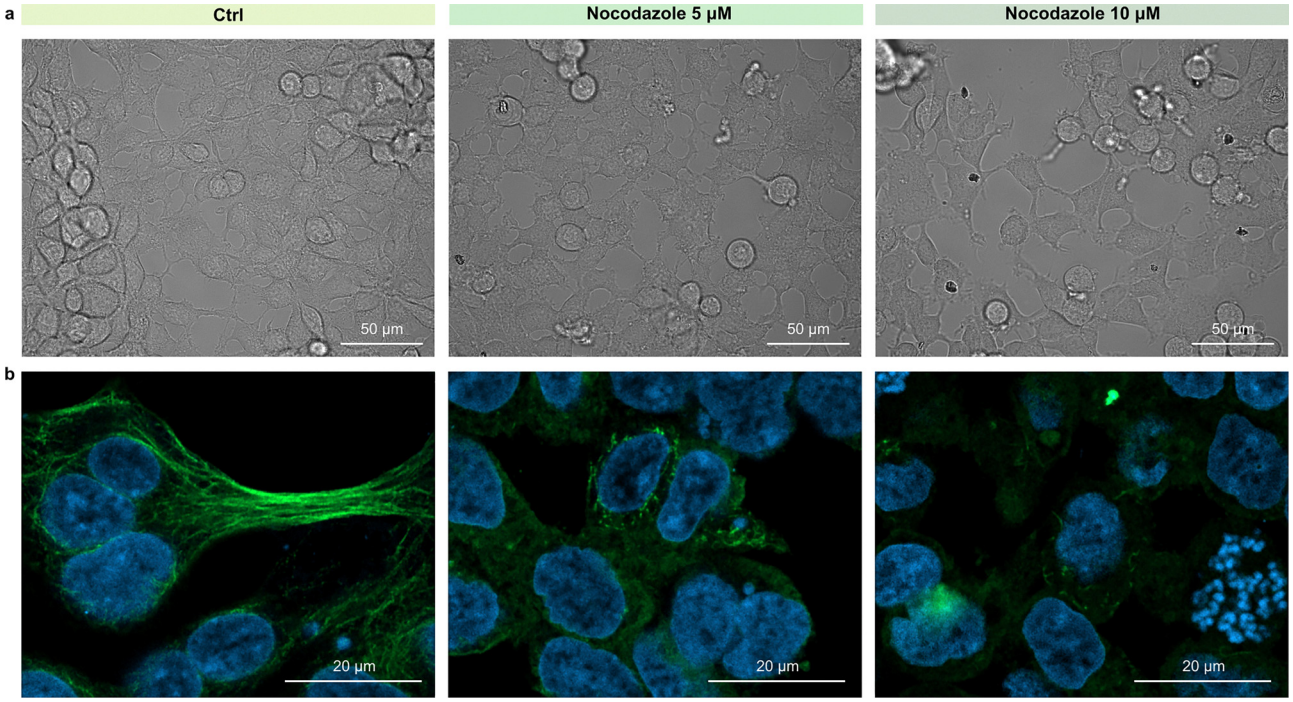

Fig. 6 Microtubule depolymerization in HEK 293 cells. (a) Brightfield images of cells not subjected to microtubule disruption (Ctrl) and of cells where microtubules have been disrupted by exposure to 5 and 10 μM nocodazole for 4 h. (b) Visualisation of the microtubule network with α-tubulin immunostaining (green) and nuclear staining (DAPI; blue).

unperturbed cells (Fig. S6). We performed the same analysis of the trajectories as for cell energy-depleted conditions, and hence have relegated some results to the supplementary information for brevity.

Qualitative inspection of the trajectories (Fig. 7a) shows that, compared to in unperturbed cells (Fig. 7a; Ctrl), most mitochondria move shorter distances and perform fewer large scale movements after microtubule disruption (Fig. 7a; Nocodazole 5 and 10 μM). However, not all mitochondria undergo the same change upon microtubule disruption, with some of them still moving longer distances, in a similar fashion as in unperturbed cells. This high heterogeneity in the motion is present for both nocodazole concentrations (5 and 10 μM).

The mean square displacement averaged over lag time for 20 randomly selected trajectories shows a modest decrease in the heterogeneity of the motion comparing unperturbed cells (Fig. 7b; Ctrl) to microtubule disrupted ones (Fig. 7b; Nocodazole 5 and 10 μM). The largest difference is an overall reduced displacement upon microtubule disruption, both for shorter and longer timescales, with no major difference between the nocodazole concentrations (5 and 10 μM). The change in motion upon microtubule disruption is clearly visible also in the ensemble- and time-averaged mean square displacement (Fig. 7c). While mitochondria in unperturbed cells move super-diffusively for most of the observed time (Fig. 7c; Ctrl), after microtubule disruption, the mean square displacement shows a slightly sub-diffusive behaviour for short time scales up to $\sim$10 s.

The displacement distribution likewise shows an overall decrease in the motion upon microtubule disruption (Fig. S11). Fits of the mathematical model originally developed to describe the motion in glassy systems still describes the data well, both in unperturbed and microtubule-disrupted cells (Fig. S11), providing the opportunity to quantify changes to the dynamics through the model parameters (Table 2). Both the waiting-time before taking a first jump, τ_1, and the waiting-time before taking a subsequent jump, τ_2, increase upon microtubule disruption, implying that microtubule-disruption causes mitochondria to wait for longer before making a jump. The extent of the rattling, l, and the length of the jumps, d, instead show far less of a variation, suggesting that the majority of the change is in the waiting times. Nevertheless, there does seem to be a decrease of both lengths upon microtubule disruption.

To support the observed change in waiting times, we again calculated the time it takes to move a given distance the first and subsequent time(s) directly from the data. We focus on a distance of 0.30 μm (Fig. 8) but present two other choices in the supplement (Fig. S12). Comparing unperturbed cells (Fig. 8; Ctrl) with cells where the microtubules have been disrupted (Fig. 8; Nocodazole 5 and 10 μM), shows a substantial increase both in the waiting time before a mitochondrion moves the distance a first time (blue data points) and a subsequent time (orange data points), in line with the results extracted from fitting (Table 2).

Summarising, disruption of microtubule fibres seems to negatively affect mitochondrial motion for long distances. Upon disruption, the mean square displacement becomes subdiffusive, in accordance with previous observations for micron-sized beads within endosomes,[75] lysosomes,[76] and

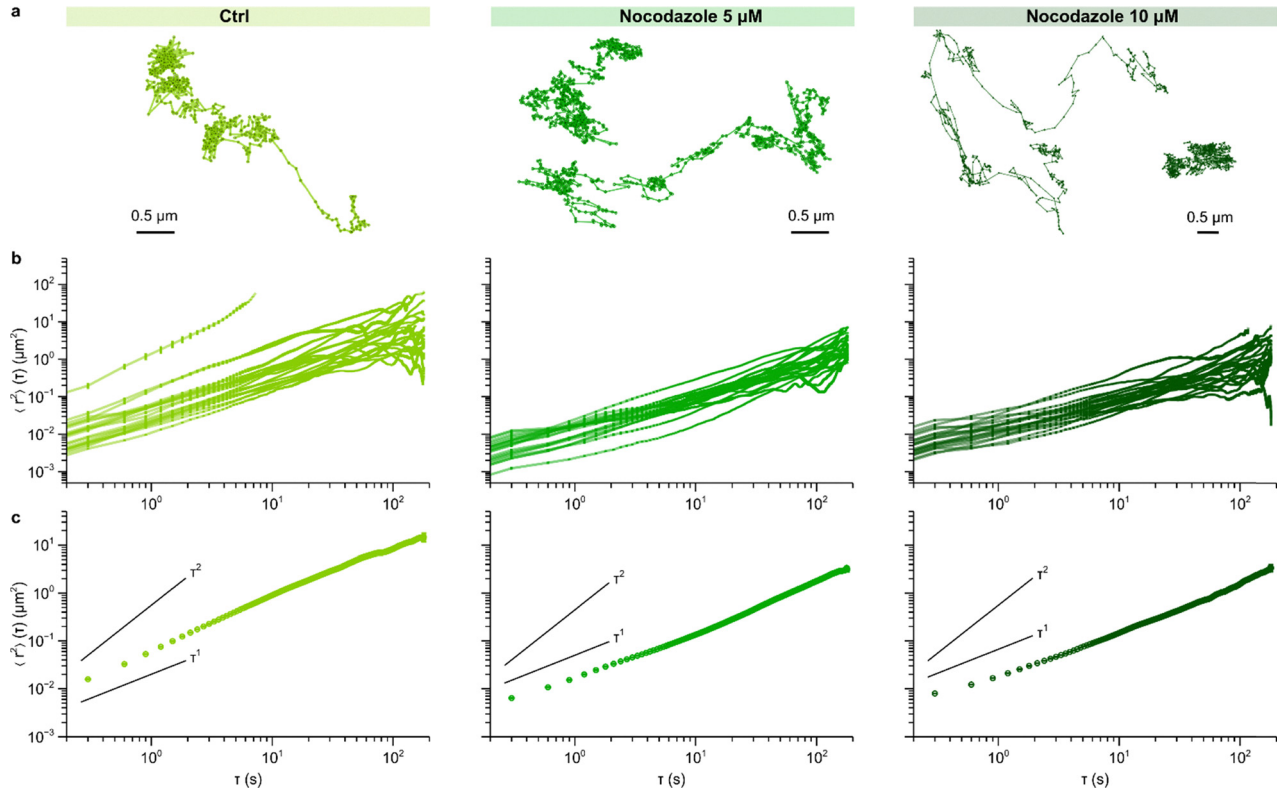

Fig. 7 Mean square displacement of mitochondria after microtubule disruption in HEK 293 cells. The results are shown for control cells (no microtubule disruption), and for cells where microtubules have been disrupted by exposure to 5 and 10 μM nocodazole for 4 h. (a) Representative examples of mitochondrial trajectories. (b) Time-averaged mean square displacement of 20 random trajectories as a function of lag time, τ. Error bars represent standard error of the mean. (c) Ensemble- and time-averaged mean square displacement of mitochondria. Error bars represent standard error of the mean (most of them too small to be visible). Solid lines represent diffusive motion (proportional to τ) and ballistic motion (proportional to τ^2), respectively, as a guide to the eye.

Table 2 Parameters describing mitochondrial motion after microtubule disruption in HEK 293 cells. The parameters were extracted by fitting a previously presented model describing the motion in several glassy systems[4,38] to the displacement distribution (Fig. S11). τ_1 denotes the time before a first jump; τ_2, the time before any subsequent jump; l, the size of the rattling; and d, the size of a jump

Condition	τ_1 (s)	τ_2 (s)	l (μm)	d (μm)
Control	1.69 ± 0.08	1.22 ± 0.19	0.072 ± 0.002	0.104 ± 0.005
5 μM nocodazole	3.81 ± 0.17	2.50 ± 0.38	0.058 ± 0.001	0.096 ± 0.003
10 μM nocodazole	2.98 ± 0.15	2.27 ± 0.28	0.062 ± 0.001	0.085 ± 0.003

macropinosomes.[76] However, the mitochondria still perform longer jumps and move longer distances, albeit less frequently than under unperturbed conditions. While the majority of microtubules are disrupted, smaller fragments still remain (Fig. 6b), so it may be that mitochondria thereby have some opportunity to move longer, explaining the presence of rare jumps. It should also be considered that microtubule disruption using nocodazole is reversible;[77] while we minimised the time between nocodazole removal and microscopy acquisition, a minor (re)polymerization might have taken place. However, previous literature reports observations of longer scale movements for nano-sized particles injected into the cytosol of cells, both under unperturbed conditions and upon microtubule disruption.[12,63] Given that nano-sized particles injected into the cytosol are very unlikely to be carried by motor proteins, these observations indicate that objects can move far also without access to motor-protein driven transport along the cytoskeleton, consistent with our observations of mitochondria moving longer distances even after microtubule disruption. Notably, while the presence of the actin network can confine mitochondria and thereby decrease their motility,[78,79] through actin-myosin contractile activity it can also stir the cytoplasm causing diffusive-like fluctuations of mitochondria.[12]

Crowding

Even if not directly involved in motor protein-driven motion, the crowded environment inside the cell could influence how organelles move.[18,19] Indeed, mammalian cells, such as the human cells used here, consist of a multitude of different macromolecules, organelles and cytoskeleton components all

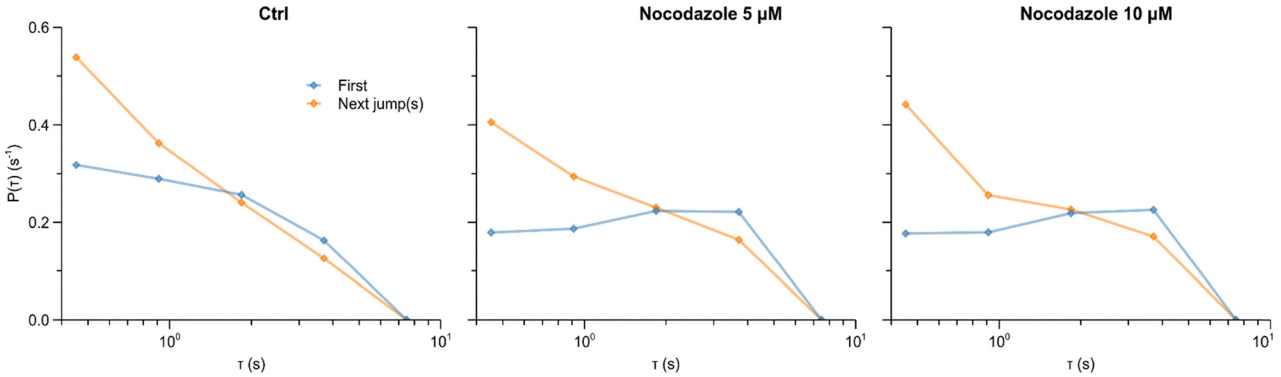

Fig. 8 Waiting time distributions of mitochondria to move a given distance in microtubule-disrupted HEK 293 cells. The time before moving a certain distance the first time (blue) and any subsequent time (orange) was evaluated for a distance of 0.30 μm (other choices of distance are shown in Fig. S12). The results are presented in terms of the normalised probability density function of the two times. Note the log scale. The calculations were limited to the first 10 s only (see Experimental section for details).

'packed' inside the cell. It has been estimated that an eukaryotic cell has around 300–400 g L^{-1} of macromolecules, meaning that up to 40% of the volume is occupied, significantly reducing the amount of free volume.[80] One should also consider that such estimates are averaged over the cell, and it is certainly possible that it is even more crowded close to a microtubule, where many different organelles all need to be transported.

In order to test the effect of crowding on mitochondrial motion, we used a different system compared to above, namely HEK 293 cells where the mitochondrial matrix has been fluorescently labelled with the fluorescent protein AcGFP1,[42,43] thereby labelling the mitochondrion itself. These cells, while derived from HEK 293 cells, are not identical to HEK 293 cells. To assess how different they are from the point of view of this work, we directly compared the movement of mitochondria in these cells with that in the 'normal' HEK 293 cells used above (unperturbed cells from the cell depletion and microtubule disruption experiments). Although there is less overlap than when the two independent datasets from 'normal' HEK 293 cells are compared with each other, there is nevertheless a substantial agreement (Fig. S6).

To alter the level of crowding, we used sorbitol, a sugar commonly used as molecular crowder,[81–83] to increase the osmotic pressure of the cell medium, that is, make the medium hypertonic. When cells are exposed to such a hypertonic solution, water is transported out of the cell, thus reducing cell volume and consequently increasing intracellular crowding. Sorbitol was added to the cell medium, in which cells were already growing, as a small volume of concentrated solution to reach a final concentration of 550 mM of sorbitol. Such a high sorbitol concentration has previously been shown to induce a substantial amount of crowding in HEK 293 cells.[83] To be sure that the crowding was due to the addition of sorbitol, and not the act of adding solution to the cells, an isotonic buffer (Phosphate-Buffered Saline; PBS) was added to a separate Petri dish with cells in the same volume as the sorbitol solution.

To confirm that the cells indeed were crowded, we observed the cells using brightfield microscopy (Fig. 9a). As expected, when sorbitol was added to the cell medium, the cells started to shrink, becoming more 'rounded', while no such effect is observed for unperturbed cells or cells where only PBS was added. To quantify the level of crowding, we measured the change in cell area, readily available from the brightfield images (Fig. 9a), which showed a roughly halving upon exposure to sorbitol (Fig. 9b). We also monitored how cell area changed with time (Fig. 9c). It is clear from these results that cell area does not change substantially over time for unperturbed cells, and also not for cells where PBS was added; in the presence of sorbitol, however, cell area decreases abruptly in the first 2 min, and progressively stabilises after around 10 min.

To follow the motion of mitochondria upon crowding, the cells were observed using fluorescence microscopy and the detached mitochondria tracked (Fig. S3 shows the trajectory length distributions). It was possible to follow cells from the same Petri dish before and after crowding, though not always the same cell, as the addition of sorbitol invariably moves the microscopy stage. Of note, increasing cell crowding necessarily pushes everything together inside the cell, thereby challenging the visualisation of the detached mitochondria, more easily hidden by the mitochondrial network, making the tracking harder than under the conditions investigated above. It also biases the results in the direction of the less crowded regions of the cell, as these are the regions where tracking detached mitochondria is easier.

Compared to non-perturbed cells (Fig. 10a; Ctrl) mitochondria under crowding exhibit more confined trajectories, but still some of them present moments of longer-scale movement (Fig. 10a; Sorbitol 550 mM). This is also reflected in the time-averaged mean square displacement of individual trajectories, where crowding largely does not seem to affect the heterogeneity among different trajectories, though the mean square displacements are overall shifted downwards as well as increase with a less steep slope (Fig. 10b). The latter is more

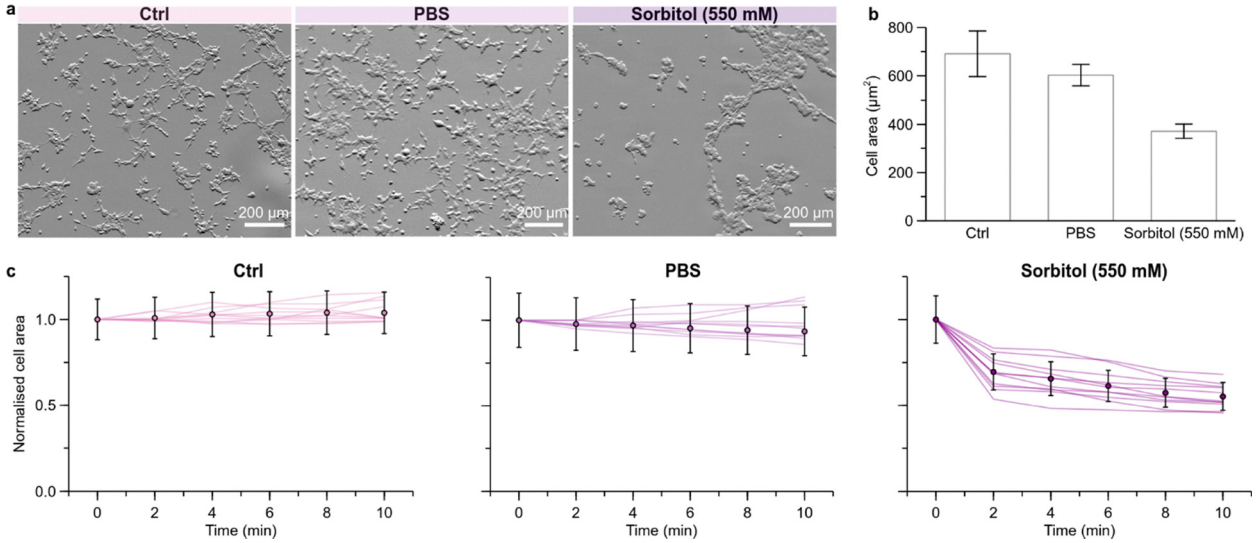

Fig. 9 Crowding in HEK 293 cells. (a) Brightfield images of cells *not* subjected to crowding (Ctrl); cells where only PBS was added (PBS); and cells crowded by exposure to 550 mM sorbitol (Sorbitol 550 mM) after 10 min of exposure and imaging. (b) Average cell area after 10 min of exposure. Data are represented as the mean ± its standard error over 35 cells per condition. (c) Cell area changes with time during the exposure. The results are presented for 11 individual cells per condition which were followed over time (lines), together with the mean ± its standard error over the same cells (datapoints). For each condition, all areas were normalised to the respective mean cell area at the beginning of the exposure.

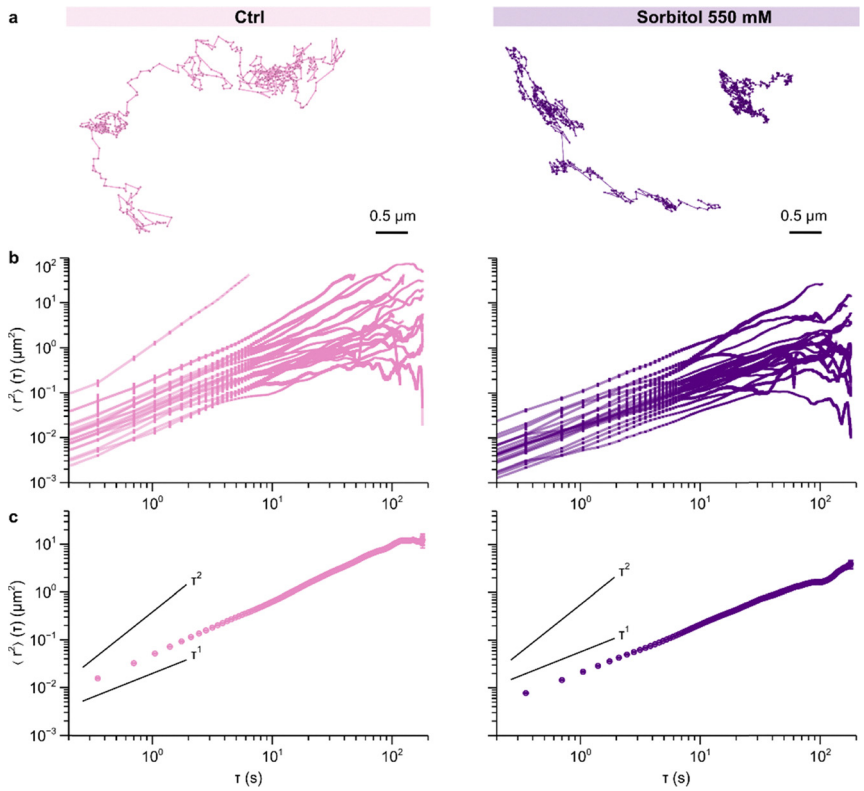

Fig. 10 Mean square displacement of mitochondria in crowded HEK 293 cells. The results are shown for control cells (not subjected to any perturbation) and for cells crowded through exposure to 550 mM sorbitol. (a) Representative examples of mitochondrial trajectories. (b) Time-averaged mean square displacement of 20 random trajectories as a function of lag time, τ. Error bars represent standard error of the mean. (c) Ensemble- and time-averaged mean square displacement of mitochondria. Error bars represent standard error of the mean (most of them too small to be visible). Solid lines represent diffusive motion (proportional to τ) and ballistic motion (proportional to τ^2), respectively, as a guide to the eye.

clear from the ensemble- and time-averaged mean square displacement, which is lowered overall but whose exponent also drops from slightly superdiffusive to slightly subdiffusive upon crowding (Fig. 10c).

Table 3 Parameters describing mitochondrial motion in crowded HEK 293 cells. The parameters were extracted by fitting a previously presented model describing the motion in several glassy systems[4,38] to the displacement distribution (Fig. S13). τ_1 denotes the time before a first jump; τ_2, the time before any subsequent jump; l, the size of the rattling; and d, the size of a jump

Condition	τ_1 (s)	τ_2 (s)	l (μm)	d (μm)
Control	2.03 ± 0.09	1.01 ± 0.17	0.077 ± 0.002	0.111 ± 0.007
550 mM sorbitol	3.27 ± 0.16	2.33 ± 0.41	0.062 ± 0.001	0.101 ± 0.004

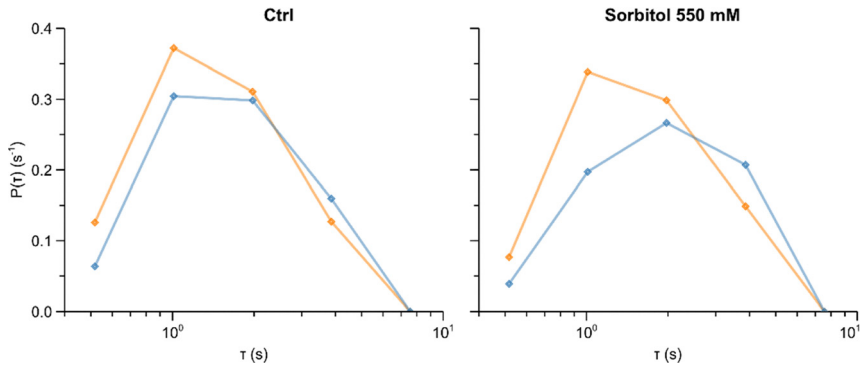

Fig. 11 Waiting time distributions of mitochondria to move a given distance in crowded HEK 293 cells. The time before moving a certain distance the first time (blue) and any subsequent time (orange) was evaluated for a distance of 0.30 μm (other choices of distance are shown in Fig. S14). The results are presented in terms of the normalised probability density function of the two times. Note the log scale. The calculations were limited to the first 10 s only (see Experimental section for details).

The displacement distribution (Fig. S13) supports the idea that mitochondria move shorter distances upon crowding. Furthermore, since the mathematical model still describes the data well, we may quantify the change of motion upon crowding through the fitting parameters (Table 3). Even though the cells are slightly different, the parameters for unperturbed cells are quite similar to those of the cells used above (Tables 1 and 2). Indeed the extent of the motion is in the range of ~0.06–0.08 μm for the rattling (l) and in the range of ~0.10–0.15 μm for the jumps (d). In terms of the effect of crowding, the extent of the rattling (l) decreases, together with a more modest decrease in the jumps (d). More prominent is the change in the timescales, where the waiting time before taking a first jump (τ_1) and the waiting time before taking a subsequent jump (τ_2) both increase upon crowding. Both of these observations are consistent with the idea that the extent of rattling decreases concurrently with an increase in the waiting time before moving longer.

To lend more weight to the observed change in waiting times, we again evaluated the distribution of waiting times before moving a certain distance directly from the trajectories, showing that mitochondria in crowded cells indeed take longer before moving (Fig. 11; Sorbitol 550 mM) regardless of the distance considered (Fig. S14).

Overall, increasing the level of cell crowding seems to have a minor effect on the motion of mitochondria. It is possible that we miss some effect of crowding specifically for motion in the vicinity of the mitochondrial network which gets very dense upon crowding and where mitochondria consequently are difficult to follow. Nevertheless, the mitochondria that we are able to follow should also experience a crowded environment, and the modest effects we observe thus suggest that the impact of crowding is less relevant compared to other factors. Nevertheless, while mitochondrial motion in crowded cells is still characterised by stalling interspersed with periods of longer movements, just like in unperturbed cells, the motion in crowded cells clearly differs. Thus the extent of the rattling appears to be lower, as evidenced both by the overall lowering of the mean square displacements (Fig. 10b and c) as well as by the modest decrease in the fitting parameter describing the extent of the rattling (l; Table 3). Furthermore, the waiting time before moving longer becomes larger upon crowding, as observed from the slower growth of the mean square displacements (Fig. 10b and c), as well as the increase in waiting times extracted from the fitting (τ_1 and τ_2; Table 3) and the direct calculation (Fig. 11). Both of these observations may be expected from crowding, as when the cellular components get pushed together, there is simply less space to rattle around as well as fewer opportunities to move longer distances. Aside from such physical constraints, it has been shown that macromolecular crowding can also more directly affect the behaviour of motor proteins[84] as well as alter the rate of polymerization/depolymerization of microtubules;[85] such effects may also contribute to the slowdown of mitochondrial motion.

Conclusions

In this work we have followed the motion of mitochondria in human cells as a model system for cargo transported by motor proteins. In particular, we subjected the system to various perturbations in order to gain quantitative insights into the

mechanisms underlying motor protein-driven motion. Thus we depleted cell energy (ATP), a key driver of motor protein-driven motion; we disrupted the microtubule network, upon which the (mitochondria-carrying) motor proteins move; and we increased cellular crowding, making the cell interior more packed. In all cases, we observed changes to the motion of mitochondria, though depending upon the perturbation, in different ways and to varying extents.

Cell energy depletion has a large effect on mitochondrial motion. Under unperturbed conditions, mitochondrial motion is characterised by moments of rattling, where the mitochondria only explore a limited region, interspersed by jumps, where the mitochondria move much longer, often in a roughly unidirectional manner. Upon cell energy depletion, the largest effect is that the waiting time before performing a jump becomes substantially longer, though there is also a decrease in the jump lengths and a more modest decrease in the extent of the rattling. One interpretation of these observations is that cell energy depletion affects the processivity of motor protein-driven motion. The extent of rattling becoming smaller upon cell energy depletion is also consistent with a diminishing of cytoskeleton fluctuations, which are also cell energy dependent. These fluctuations can also drive longer scale movements,[12,63] and their decline upon cell energy depletion could also play a wider role.

Disruption of the microtubules, instead, has a smaller effect on mitochondrial motion. Again, the largest difference appears to be in the waiting time, but in this case it only increases by a factor of 2 or so upon microtubule disruption, with no major difference in the extent of rattling or the lengths of longer scale movements. While the presence of longer-scale movements in the absence of microtubules may seem surprising, such movements have previously been observed also for objects not carried by motor proteins,[12,63] probably driven by intracellular fluctuations, including of the (remaining part of the) cytoskeleton.

Finally, the effect of increased crowding also has a rather small effect. This seems to be driven by both an increase, at the most by a factor of 2, in the waiting time, together with a modest decrease in the extent of the rattling, upon crowding. These observations are consistent with crowding causing fewer opportunities for longer scale movements, thereby increasing the waiting time, but also making the cell interior more dense, decreasing the extent of the rattling.

Overall, our observations illustrate that motor protein-driven motion is mechanistically highly complex. Nevertheless, in all cases, the largest change upon perturbation of the system appears to be in the waiting times. This suggests that the picture of motor protein-driven motion constituting a combination of rattling mixed with infrequent jumps provides a useful framework for understanding the motion and, in particular, underscores the importance of the transition between rattling and jumping.

Author contributions

B. C.: investigation, writing – original draft. W. J. H. K.: resources, writing – review & editing. A. M. D.: resources, supervision, writing – review & editing. C. Å.: conceptualization, supervision, writing – original draft.

Conflicts of interest

There are no conflicts to declare.

Data availability

The data supporting the conclusions drawn in this manuscript are contained within the article and supplementary information (SI). Further inquiries may be directed to the corresponding author. Supplementary information: extended experimental results. See DOI: https://doi.org/10.1039/d5sm01174d.

Acknowledgements

B. C. was supported by a scholarship awarded under the Advanced Materials theme of the Faculty of Science and Engineering, University of Groningen. The microscopy was performed at the University Medical Center Groningen Imaging and Microscopy Center. We thank A. Salvati (University of Groningen, Groningen, The Netherlands) for providing the HEK 293 cells as well as nocodazole and sodium azide, and A. P. Nagelkerke (University of Groningen, Groningen, The Netherlands) for providing antibodies for tubulin immunostaining. For help with the ATP assay we thank I. A. M. de Graaf and E. Post (University of Groningen, Groningen, The Netherlands).

Notes and references

1 B. Alberts, A. Johnson, J. Lewis, M. Raff, K. Roberts and P. Walter, *Molecular biology of the cell*, Garland Science, New York, 5th edn, 2008, pp. 965–1052.
2 K. Barlan and V. I. Gelfand, *Cold Spring Harbor Perspect. Biol.*, 2017, **9**, a025817.
3 W. O. Hancock, *Nat. Rev. Mol. Cell Biol.*, 2014, **15**, 615–628.
4 P. Chaudhuri, L. Berthier and W. Kob, *Phys. Rev. Lett.*, 2007, **99**, 060604.
5 M. P. Ciamarra, R. Pastore and A. Coniglio, *Soft Matter*, 2015, **12**, 358–366.
6 B. R. Parry, I. V. Surovtsev, M. T. Cabeen, C. S. O'Hern, E. R. Dufresne and C. Jacobs-Wagner, *Cell*, 2014, **156**, 183–194.
7 M. C. Munder, D. Midtvedt, T. Franzmann, E. Nüske, O. Otto, M. Herbig, E. Ulbricht, P. Müller, A. Taubenberger, S. Maharana, L. Malinovska, D. Richter, J. Guck, V. Zaburdaev and S. Alberti, *eLife*, 2016, **5**, e09347.
8 C. Åberg and B. Poolman, *Biophys. J.*, 2021, **120**, 2355–2366.
9 N. Schramma, C. Perugachi Israëls and M. Jalaal, *Proc. Natl. Acad. Sci. U. S. A.*, 2023, **120**, e2216497120.
10 B. Corci, O. Hooiveld, A. M. Dolga and C. Åberg, *Soft Matter*, 2023, **19**, 2529–2538.

11 H. Salman, Y. Gil, R. Granek and M. Elbaum, *Chem. Phys.*, 2002, **284**, 389–397.
12 M. Guo, A. J. Ehrlicher, M. H. Jensen, M. Renz, J. R. Moore, R. D. Goldman, J. Lippincott-Schwartz, F. C. Mackintosh and D. A. Weitz, *Cell*, 2014, **158**, 822–832.
13 W. Xu, E. Alizadeh and A. Prasad, *Biophys. J.*, 2018, **114**, 2933–2944.
14 E. S. Nadezhdina, A. J. Lomakin, A. A. Shpilman, E. M. Chudinova and P. A. Ivanov, *Biochim. Biophys. Acta, Mol. Cell Res.*, 2010, **1803**, 361–371.
15 S. C. Leary, B. C. Hill, C. N. Lyons, C. G. Carlson, D. Michaud, C. S. Kraft, K. Ko, D. M. Glerum and C. D. Moyes, *J. Biol. Chem.*, 2002, **277**, 11321–11328.
16 C. Dumontet and M. A. Jordan, *Nat. Rev. Drug Discovery*, 2010, **9**, 790–803.
17 R. J. Ellis, *Curr. Opin. Struct. Biol.*, 2001, **11**, 114–119.
18 M. A. Mourão, J. B. Hakim and S. Schnell, *Biophys. J.*, 2014, **107**, 2761–2766.
19 F. Höfling and T. Franosch, *Rep. Prog. Phys.*, 2013, **76**, 046602.
20 V. Sabharwal and S. P. Koushika, *Front. Cell. Neurosci.*, 2019, **13**, 470.
21 L. D. Osellame, T. S. Blacker and M. R. Duchen, *Best Pract. Res., Clin. Endocrinol. Metab.*, 2012, **26**, 711–723.
22 M. Picard and O. S. Shirihai, *Cell Metab.*, 2022, **34**, 1620–1653.
23 E. P. Bulthuis, M. J. W. Adjobo-Hermans, P. H. G. M. Willems and W. J. H. Koopman, *Antioxid. Redox Signal.*, 2019, **30**, 2066–2109.
24 B. Glancy, Y. Kim, P. Katti and T. B. Willingham, *Front. Physiol.*, 2020, **11**, 541040.
25 T. Liu, T. Stephan, P. Chen, J. Keller-Findeisen, J. Chen, D. Riedel, Z. Yang, S. Jakobs and Z. Chen, *Proc. Natl. Acad. Sci. U. S. A.*, 2022, **119**, e2215799119.
26 L. Tilokani, S. Nagashima, V. Paupe and J. Prudent, *Essays Biochem.*, 2018, **62**, 341–360.
27 N. Zamponi, E. Zamponi, S. A. Cannas, O. V. Billoni, P. R. Helguera and D. R. Chialvo, *Sci. Rep.*, 2018, **8**, 363.
28 A. S. Moore and E. L. Holzbaur, *Curr. Opin. Physiol.*, 2018, **3**, 94–100.
29 A. Melkov and U. Abdu, *Cell. Mol. Life Sci.*, 2018, **75**, 163–176.
30 M. J. I. Müller, S. Klumpp and R. Lipowsky, *Proc. Natl. Acad. Sci. U. S. A.*, 2008, **105**, 4609–4614.
31 K. Rezaul, D. Gupta, I. Semenova, K. Ikeda, P. Kraikivski, J. Yu, A. Cowan, I. Zaliapin and V. Rodionov, *Traffic*, 2016, **17**, 475–486.
32 O. Osunbayo, J. Butterfield, J. Bergman, L. Mershon, V. Rodionov and M. Vershinin, *Biophys. J.*, 2015, **108**, 1480–1483.
33 M. Tjioe, S. Shukla, R. Vaidya, A. Troitskaia, C. S. Bookwalter, K. M. Trybus, Y. R. Chemla and P. R. Selvin, *eLife*, 2019, **8**, e50974.
34 C. A. Schneider, W. S. Rasband and K. W. Eliceiri, *Nat. Methods*, 2012, **9**, 671–675.
35 J. Schindelin, I. Arganda-Carreras, E. Frise, V. Kaynig, M. Longair, T. Pietzsch, S. Preibisch, C. Rueden, S. Saalfeld, B. Schmid, J.-Y. Tinevez, D. J. White, V. Hartenstein, K. Eliceiri, P. Tomancak and A. Cardona, *Nat. Methods*, 2012, **9**, 676–682.
36 J.-Y. Tinevez, N. Perry, J. Schindelin, G. M. Hoopes, G. D. Reynolds, E. Laplantine, S. Y. Bednarek, S. L. Shorte and K. W. Eliceiri, *Methods*, 2017, **115**, 80–90.
37 D. Ershov, M.-S. Phan, J. W. Pylvänäinen, S. U. Rigaud, L. Le Blanc, A. Charles-Orszag, J. R. W. Conway, R. F. Laine, N. H. Roy, D. Bonazzi, G. Duménil, G. Jacquemet and J.-Y. Tinevez, *Nat. Methods*, 2022, **19**, 829–832.
38 P. Chaudhuri, Y. Gao, L. Berthier, M. Kilfoil and W. Kob, *J. Phys.: Condens. Matter*, 2008, **20**, 244126.
39 B. Wang, S. M. Anthony, S. C. Bae and S. Granick, *Proc. Natl. Acad. Sci. U. S. A.*, 2009, **106**, 15160–15164.
40 M. Shah, L. A. Chacko, J. P. Joseph and V. Ananthanarayanan, *Cell. Mol. Life Sci.*, 2021, **78**, 3969–3986.
41 A. R. Fenton, T. A. Jongens and E. L. F. Holzbaur, *Nat. Commun.*, 2021, **12**, 4578.
42 C. E. J. Dieteren, P. H. G. M. Willems, R. O. Vogel, H. G. Swarts, J. Fransen, R. Roepman, G. Crienen, J. A. M. Smeitink, L. G. J. Nijtmans and W. J. H. Koopman, *J. Biol. Chem.*, 2008, **283**, 34753–34761.
43 C. E. J. Dieteren, S. C. A. M. Gielen, L. G. J. Nijtmans, J. A. M. Smeitink, H. G. Swarts, R. Brock, P. H. G. M. Willems and W. J. H. Koopman, *Proc. Natl. Acad. Sci. U. S. A.*, 2011, **108**, 8657–8662.
44 L.-P. Chen, Y.-P. Wei and Q. Tian, *Alzheimers Dement.*, 2015, **11**, P367–P367.
45 T. Savin and P. S. Doyle, *Biophys. J.*, 2005, **88**, 623–638.
46 X. Michalet, *Phys. Rev. E:Stat., Nonlinear, Soft Matter Phys.*, 2010, **82**, 041914.
47 A. A. Astafiev, A. M. Shakhov, A. A. Osychenko, M. S. Syrchina, A. V. Karmenyan, U. A. Tochilo and V. A. Nadtochenko, *ACS Omega*, 2020, **5**, 12527–12538.
48 D. Holcman, P. Parutto, J. E. Chambers, M. Fantham, L. J. Young, S. J. Marciniak, C. F. Kaminski, D. Ron and E. Avezov, *Nat. Cell Biol.*, 2018, **20**, 1118–1125.
49 S. C. Weber, A. J. Spakowitz and J. A. Theriot, *Proc. Natl. Acad. Sci. U. S. A.*, 2012, **109**, 7338–7343.
50 T. Ishikawa, B.-L. Zhu and H. Maeda, *Toxicol. Ind. Health*, 2006, **22**, 337–341.
51 K. Neikirk, A. G. Marshall, B. Kula, N. Smith, S. LeBlanc and A. Hinton, *Eur. J. Cell Biol.*, 2023, **102**, 151371.
52 L. Berthier, G. Biroli, J.-P. Bouchaud, W. Kob, K. Miyazaki and D. R. Reichman, *J. Chem. Phys.*, 2007, **126**, 184503.
53 L. Berthier, G. Biroli, J.-P. Bouchaud, W. Kob, K. Miyazaki and D. R. Reichman, *J. Chem. Phys.*, 2007, **126**, 184504.
54 L. Berthier and W. Kob, *J. Phys.: Condens. Matter*, 2007, **19**, 205130.
55 E. R. Weeks, J. C. Crocker, A. C. Levitt, A. Schofield and D. A. Weitz, *Science*, 2000, **287**, 627–631.
56 G. Marty and O. Dauchot, *Phys. Rev. Lett.*, 2005, **94**, 015701.
57 E. W. Montroll and G. H. Weiss, *J. Math. Phys.*, 1965, **6**, 167–181.
58 B. D. Hughes, *Random walks and random environments: Random walks*, Clarendon Press, Oxford, 1995, vol. 1, pp. 241–328.

59 L. O. Hedges, L. Maibaum, D. Chandler and J. P. Garrahan, *J. Chem. Phys.*, 2007, **127**, 211101.
60 Y. Jung, J. P. Garrahan and D. Chandler, *Phys. Rev. E:Stat., Nonlinear, Soft Matter Phys.*, 2004, **69**, 061205.
61 C. Appert-Rolland, M. Ebbinghaus and L. Santen, *Phys. Rep.*, 2015, **593**, 1–59.
62 C. Kural, H. Kim, S. Syed, G. Goshima, V. I. Gelfand and P. R. Selvin, *Science*, 2005, **308**, 1469–1472.
63 P. Witzel, M. Götz, Y. Lanoiselée, T. Franosch, D. S. Grebenkov and D. Heinrich, *Biophys. J.*, 2019, **117**, 203–213.
64 O. A. Quintero, M. M. DiVito, R. C. Adikes, M. B. Kortan, L. B. Case, A. J. Lier, N. S. Panaretos, S. Q. Slater, M. Rengarajan, M. Feliu and R. E. Cheney, *Curr. Biol.*, 2009, **19**, 2008–2013.
65 K. Majstrowicz, U. Honnert, P. Nikolaus, V. Schwarz, S. J. Oeding, S. A. Hemkemeyer and M. Bähler, *J. Cell Sci.*, 2021, **134**, jcs255844.
66 O. Sato, T. Sakai, Y. Choo, R. Ikebe, T. M. Watanabe and M. Ikebe, *J. Biol. Chem.*, 2022, **298**, 101883.
67 S. Li, S. Xu, B. A. Roelofs, L. Boyman, W. J. Lederer, H. Sesaki and M. Karbowski, *J. Cell Biol.*, 2014, **208**, 109–123.
68 A. S. Moore, Y. C. Wong, C. L. Simpson and E. L. F. Holzbaur, *Nat. Commun.*, 2016, **7**, 12886.
69 C. Yang and T. M. Svitkina, *Nat. Cell Biol.*, 2019, **21**, 603–613.
70 A. S. Moore, S. M. Coscia, C. L. Simpson, F. E. Ortega, E. C. Wait, J. M. Heddleston, J. J. Nirschl, C. J. Obara, P. Guedes-Dias, C. A. Boecker, T.-L. Chew, J. A. Theriot, J. Lippincott-Schwartz and E. L. F. Holzbaur, *Nature*, 2021, **591**, 659–664.
71 B. Cunniff, A. J. McKenzie, N. H. Heintz and A. K. Howe, *Mol. Biol. Cell*, 2016, **27**, 2662–2674.
72 S. Madan, B. Uttekar, S. Chowdhary and R. Rikhy, *Front. Cell Dev. Biol.*, 2022, **9**, 781933.
73 J. Hoebeke, G. Van Nijen and M. De Brabander, *Biochem. Biophys. Res. Commun.*, 1976, **69**, 319–324.
74 V. Čermák, V. Dostál, M. Jelínek, L. Libusová, J. Kovář, D. Rösel and J. Brábek, *Eur. J. Cell Biol.*, 2020, **99**, 151075.
75 J. Mahowald, D. Arcizet and D. Heinrich, *Chem. Phys. Chem.*, 2009, **10**, 1559–1566.
76 L. Digiacomo, F. D'Autilia, W. Durso, P. M. Tentori, G. Caracciolo and F. Cardarelli, *Sci. Rep.*, 2017, **7**, 14836.
77 M. J. De Brabander, R. M. L. Van de Velre, F. E. M. Aerts, M. Borgers and P. A. J. Janssen, *Cancer Res.*, 1976, **36**, 905–916.
78 S.-R. Jung, J. B. Seo, D. Shim, B. Hille and D.-S. Koh, *Cell Calcium*, 2012, **51**, 459–469.
79 A. B. Fernández Casafuz, A. M. Brigante, M. C. De Rossi, A. G. Monastra and L. Bruno, *Sci. Rep.*, 2024, **14**, 23914.
80 R. J. Ellis and A. P. Minton, *Nature*, 2003, **425**, 27–28.
81 H. Cheng, J. Kartenbeck, K. Kabsch, X. Mao, M. Marqués and A. Alonso, *J. Cell. Physiol.*, 2002, **192**, 234–243.
82 A. Zagórska, E. Pozo-Guisado, J. Boudeau, A. C. Vitari, F. H. Rafiqi, J. Thastrup, M. Deak, D. G. Campbell, N. A. Morrice, A. R. Prescott and D. R. Alessi, *J. Cell Biol.*, 2006, **176**, 89–100.
83 A. J. Boersma, I. S. Zuhorn and B. Poolman, *Nat. Methods*, 2015, **12**, 227–229.
84 G. Nettesheim, I. Nabti, C. U. Murade, G. R. Jaffe, S. J. King and G. T. Shubeita, *Nat. Phys.*, 2020, **16**, 1144–1151.
85 A. T. Molines, J. Lemière, M. Gazzola, I. E. Steinmark, C. H. Edrington, C.-T. Hsu, P. Real-Calderon, K. Suhling, G. Goshima, L. J. Holt, M. Thery, G. J. Brouhard and F. Chang, *Dev. Cell*, 2022, **57**, 466–479.e6.